Mechanical Engineering Advances 2025, 3(3), 1888.
doi: https://doi.org/10.59400/mea1888

Review

Advancement of ECAPed on the thermal stability of strain hardening behaviour and conductivity in an AA5083 under thermal effect

Nagendra Singh[1,2,*], **Manoj Kumar Agrawal**[1]

[1] Department of Mechanical Engineering, GLA University, Mathura UP-281406, India

[2] Department of Mechanical Engineering, Institute of Engineering and Technology, Khandari Campus, Agra UP-282002, India

*** Corresponding author:** Nagendra Singh, singh.mech2008@gmail.com

CITATION

Singh N, Agrawal MK. Advancement of ECAPed on the thermal stability of strain hardening behaviour and conductivity in an AA5083 under thermal effect. Mechanical Engineering Advances. 2025; 3(3): 1888. https://doi.org/10.59400/mea1888

ARTICLE INFO

Received: 17 October 2024
Revised: 14 April 2025
Accepted: 18 April 2025
Available online: 16 August 2025

Abstract: The plastic distortion of AA5083 after the ECAP (Equal Channel Angular Pressing) process was found under stress at a thermal limit from 6.2 to 420 K. The EBSD (Electron Backscatter Diffraction) method was used to investigate the microstructure changes during loading, such as the kernel average misorientation mappings and orientation. The microstructure is distinguished by grains with many dislocations and small misorientation angles. When a piece is deformed at 130 K, the density of deformation faults increases at 310 K and then decreases. The yield strength mentioned thermal sensitivity shows that thermal energy starts the plastic deformation. A reduction in the removal of dislocations because of a reduction in atomic movement and an increase in increased flexibility, followed by a faster rate of strain hardening and durability of polycrystals as the temperature drops. The investigation of stress-strain graphs and the evolution of microstructure show that the thermally induced process is dominant at less than 185 K. The activity of recovery processes has increased. The aim of this study is to examine the process of applying severe plastic deformation techniques, namely equal channel angular pressing, to achieve a nanoscale structure in AA5083. The effects of applying equal channel angular pressing on the microstructure and mechanical characteristics of AA5083 were investigated. Scanning electron microscopy was employed to analyze the changes in microstructure resulting from various thermal treatments applied to the material subjected to severe plastic deformation through this process. Furthermore, a more profound comprehension of the modifications in the mechanical characteristics of this aluminum alloy was obtained.

Keywords: AA5083; ECAP; elastic anisotropy; strain hardening

1. Introduction

In this paper, because of their strong mechanical characteristics, materials with extremely metallic grains generated through intense plastic distortion are appealing. The microscopic granule size, in addition to the unique behavior of boundaries, defines such features. Such materials include substantial internal stresses that have a considerable impact on their flexibility and strength because of the non-equilibrium grain boundaries. Because of insufficient density, high resistance to corrosion, exceptional formability, and lower price, the AA5083 series has great potential for use in aerospace, automotive, and aviation applications [1]. The study of the link between solid structure and mechanical characteristics is quite interested in such sub-microcrystalline materials. It is well known that at medium temperatures, SPD materials with grain sizes greater than 110 nm retain

their deformation of plastic [1]. The natural tendency of traditional coarse-grained materials to break. The sources are the grain boundaries, sinks, and obstacles that prevent dislocations, which specifically alter the mechanics of dislocation formation and motion in SPD materials. Plastic deformity mechanisms of microgranular and nanostructured materials have been established to It is possible to perform the typical sliding of lattice dislocations inside grains using deformation of plastic. The reasons for GB sliding include grain revolving stress-induced shows in **Figure 1** [2]. It is necessary to conduct studies of thermal effects between 6.2 and 420 K since the activity of different deformations of plastic mechanisms is temperature and microstructure dependent [2].

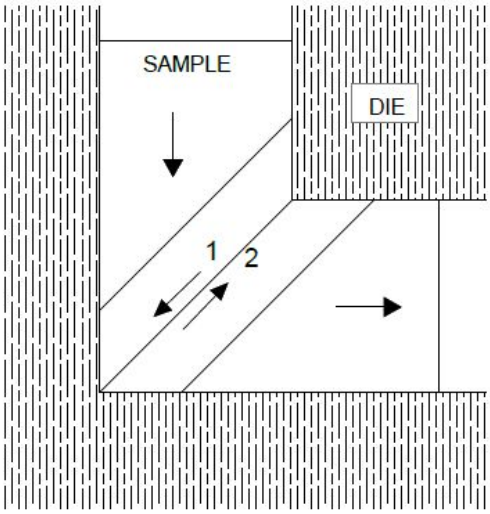

Figure 1. ECAP die geometry with sample [3].

The extremely modest temperature range where diffusion techniques can be impeded is included. There is research focused on investigating the flexibility of metals with ultrafine grains and whether they retain their strength through studies conducted at low temperatures [3]. This endeavor represents a continuation of the series of studies aimed at exploring segments and subsections of the metallic alloy AA5083. The mechanisms of thermally induced plasticity at different temperature ranges [4]. The focus is on studying the initial microstructure and how it changes as selected materials undergo plastic tensile deformation at low temperatures [4].

This applies specifically to materials that have been subjected to distortion. SPD techniques for difficult-to-work substances are resulting in advanced form and system design [5]. Bulk materials for industrial and biological purposes can be produced using ECAP [5]. Using this technique, a polycrystalline material billet is extruded through a die that has two identically cross-sectioned channels that intersect at an angle of 90° (see **Figure 2**). The cross-section of the processed materials does not significantly change because the cross-sectional areas of the two die channels are comparable. The ECAP process can be iteratively applied to the same billet, thereby achieving $\varepsilon \gg 1$. It is feasible to apply severe plastic deformation techniques, such as equal channel angular pressing, to increase the strength of aluminum alloys [6]. In this recent research, AA5083 is under investigation because thermal treatments are ineffective in strengthening this particular alloy [6].

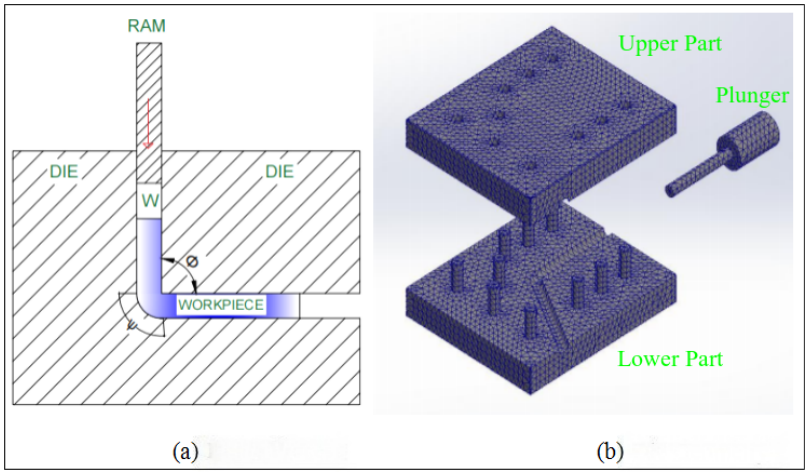

Figure 2. **(a)** The ECAP process; **(b)** finite element method simulation of the ECAP procedure and the dies employed in ECAP [7].

The ECAP method imparts a more uniform deformation and enables the production of larger-sized parts. Therefore, the final section or thickness would need to be lowered to the point where it would limit the materials' use as structural elements in processing in order to reach equivalent levels of plastic strain as attained with ECAP. Grain refining to submicrometric or even nanometric levels can be achieved with the ECAP method. The reduction in grain size leads to an enhancement in the mechanical properties of the processed material, and the material may even exhibit superplastic behavior. During the ECAP processing, a fresh crystalline lattice with submicrometric and nanometric features replaces the material's original microstructure [8]. As a result of the material's high dislocation density [8]. The subgrains in this new lattice are smaller and might be more equiaxially shaped than the original grains. The mechanical characteristics of the produced material can be changed by thermal treatments to satisfy certain operational needs. The ECAP process has been extensively researched with lightweight alloys. This research investigates the impact of applying stress to a billet that has undergone prior deformation through ECAP using two passes with a specific route B_C, during a thermal treatment at 590 K.

The stability of the microstructure of highly damaged aluminum alloys at temperatures higher than room temperature presents a difficulty [7]. An increase in the annealing temperature corresponds to a greater decline in the mechanical properties of the material. Grain size increases are followed by a decrease in mechanical attributes like yield stress. Simulations using the finite element method were used to investigate the effects of different die geometries and angle combinations [9]. Moreover, various frictional conditions and different operational temperatures were considered. Various factors, including superplasticity, grain refinement, and hardness, were correlated with the number of passes [9]. As a result, the cross-sectional distribution of the cumulative plastic strain was ascertained.

The author emphasizes the sample's structural refinement and hardness using optical and scanning electron microscopy, as well as X-ray diffraction. The formation of subgrains enclosed by high-angle borders is linked to this phenomenon. The impact of different thermal treatments on the microstructure evolution and mechanical property

changes of AA5083 after ECAP is only partially explored in a small number of studies. The objective of this current research is to enhance understanding of the behavior of this alloy following plastic deformation through ECAP and structural modification, employing diverse thermal treatments.

2. Experimental material and procedure

From there as-cast state, the ingots were formed into 10 mm diameter cylindrical bars using a machine. The bars were treated using the ECAP approach at room temperature. After six ECAP passes, the billet's final diameter and length were 10 mm and 50 mm, respectively. A total of 7.2 equivalent plastic deformations were accumulated. More information regarding the processing of AA5083 by ECAP is available, and Supplementary A depicts the whole scheme processing of ECAP [10]. The ECAP billets for tensile tests, electrical spark erosion, and stamping were used for regulating the set temperature, which was used to reach intermediate temperatures. It allowed for a 0.8 K accuracy in temperature maintenance [10]. The stress relaxation method was used to test the sensitivity to strain rate in the temperature range of 79–410 K.

The logarithmic law was used to approximate the relationship curves $\nabla\sigma_t(t)$ at time t = 110 s while taking relaxation hardening into account [11]. The approximation results at a specific temperature were used to estimate the activation volume of plastic deformation [11]. The center portion of dog bone samples that have undergone deformity is being analyzed for microstructure development. Investigation was conducted in the areas using SiC paper and diamond pastes. The samples were physically polished in ethanol to a particle size of 1.2 μm for microstructure inspection. The ECAP process channel angle $\Phi = 90^{\circ}$ and corner angle $\Psi = 0^{\circ}$ parameters have a 10 mm channel diameter. Applying the processing path employing four die passes and a pressing speed of 0.15 mm/s. Where precise experimental and processing information is provided, the general process was the same. In order to measure the EBSD and analyze the thermomechanical and elasticity properties of the ECAPed material afterwards. 2.2 h were spent at different temperatures (457 ℃, 610 ℃, and 910 ℃) in an argon atmosphere [12]. A plane parallel to the direction of extrusion was used to cut the samples.

The room temperature sample mapping step was 55 nm, the 457 ℃ sample's mapping step was 110 nm, and the 610 ℃ and 910 ℃ samples were at a certain temperature to more precisely observe peak position in the direct pole [12]. The insert direction was rotated by 90° around the EBSD data sets. The average grain diameter values may slightly rise as a result of this. The numbers given for the RT and 457 ℃ samples are overestimated because of the size of the unrecrystallized areas and the area of surface that EBSD was unable to index.

The highest load that could be applied was 5.5 N at around HV 0.8. This load ensures that there are enough substantial indentations to cover a significant number of grains and produce values that are indicative of the material in a certain direction [13]. In a nanoindentation experiment, experiments were carried out to determine the indentation modulus. The ID-TD plane of a polished surface was used for all microhardness and nanoindentation investigations mentioned in **Figure 3**. Mechanical properties of the

ECAPed material were examined in the ID direction to look at its anisotropy. Each cuboid in the AA5083 in its as-received state had a long axis that was either parallel to or perpendicular to the AA5083's axis.

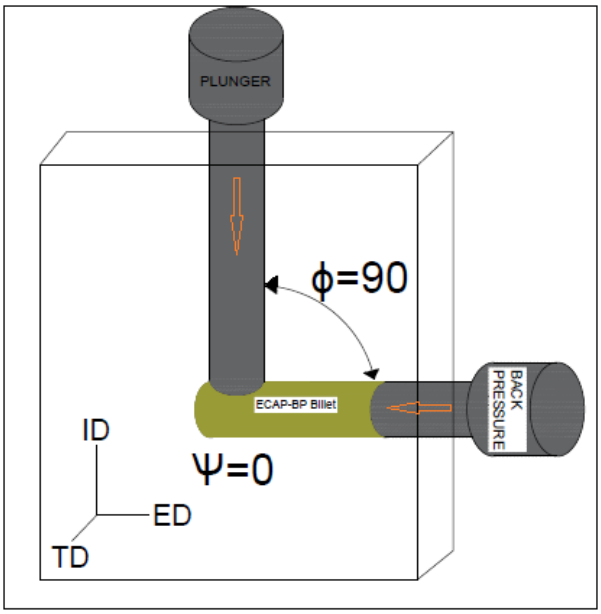

Figure 3. Schematic diagram of the ECAP die with various parameters [14].

In all experiments, a consistent extrusion velocity of 55 mm/min was utilized. The aluminum billets had a circular cross-section measuring 10 mm in diameter and 50 mm in length. Molybdenum disulfide was the lubricant employed for the execution of the ECAP process. When subjecting the same billet to multiple ECAP processes, various routes can be employed. Die geometries with an intersection angle of 90° and equal fillet radii of 2.15 mm. This geometry is depicted in **Figure 4**. Three conditions were applied to the material examination: no ECAP processing and up to two ECAP processing using route C.

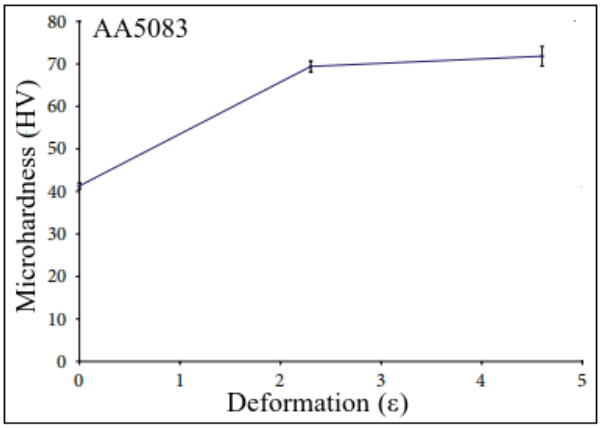

Figure 4. Hardness of the AA5083 for single and double ECAP route C passes. The hardness of AA5083 for single and double passes through the ECAP route [15].

These three material conditions were analyzed through the execution of both tensile tests and microhardness tests [15]. Ten random measurements were taken across the cross-section of the samples to evaluate each hardness value. Each indentation cycle consists of a 3 s charging time, followed by a 10 s period of maintaining charge,

and finally, a 3 s discharge. Every state of the material was subjected to tensile tests, and each state was tested three times. During the test, the tensile force increased at a rate of 112 N/s. A round ECAP billet with a cross-section of 10 mm in diameter and 50 mm in length served as the basis for the tensile billets' machining. Using a metallographic saw, the samples were sliced in order to investigate their microstructure. The samples were then ground using diamond and colloidal silica abrasives after being implanted in a non-conductive acrylic resin. For optical microscopy, the Barker electrolytic etching (2.8% HBF4) method was employed as it enables the observation of the microstructure under polarized light. A high-resolution field emission electron microscope that included secondary and backscattered electron detectors in addition to electron backscattered diffraction was the instrument utilized.

3. Experimental results

3.1. Results for low temperature plasticity

3.1.1. Tensile test

Tensile loading is applied to the microcrystalline AA5083 curves of true stress-true strain for different deformity temperatures. It is evident that when temperature decreases, flow stress rises. The relationship between plasticity and temperature is nonmonotonic; temperature has a significant impact on the curve's shape. At temperatures between 6.2 and 420 K, the maximum plasticity of around 28% is seen, and the lowest plasticity of about 3% is found close to 200 K to 420 K [16]. The result of dynamic deformation aging in alloys is thought to be the cause of the yield point occurrence on the deformity curve [16]. Dislocations start under more stress than what is needed for their future migration. The investigation into the elastic limit phenomenon in UFG polycrystals also delved into how dislocation sinks influenced this phenomenon. The sweep by a movable dislocation area A should decrease when the number of dislocation sinks increases as a result of severe plastic deformation caused by lengthening borders and subboundaries. The tensile curves exhibit a single macroscopic stress jump, which is typical of aluminum and its alloys. In this instance, the jump is separated by smooth deformation areas.

Figure 5 depicts the strain hardening coefficient of response to temperature and deformation [17]. It is evident that the coefficient of hardening of strain varies with different temperatures, decreasing monotonically. At cryogenic temperatures of 6.9 and 79 K, a high rate of hardening is active, and softening is seen in the range of 128–310 K. The yield point phenomenon is absent from the deformity curves for specimens deformed at 310 K [18]. The alloy softens quickly even at 128 K and has little ductility, which is unusual for materials at low temperatures [18].

Temperature has a significant impact on the dislocation buildup and destruction processes, which control how hard a material becomes and how plastic it remains [19]. Due to the unique behavior of the hardening coefficient shown in **Figure 6**, the temperature range between 128 and 310 K is of interest. The characteristics of the AA5083 are hardening and softening at low and high temperatures. The insert compares the temperature effects on the standard yield strength of microcrystalline AA5083 samples to that of other

alloys with the same concentration. It is clear that ECAP's microcrystalline samples have much better yield strengths than coarse-grained polycrystal samples do. The yielding strength of microcrystalline at different temperatures above 160 K is temperature dependent. In the range of 410–87 K, the elastic strength of the microcrystalline specimen increases monotonically. But the curve slope decreases. In the extremely low temperature range of 79–5.2 K, the yield strength values essentially remain constant with temperature [20]. Many metals and alloys exhibit this kind of unusual behavior in their yield strength at temperatures lower than 79 K. Not just for coarse-grained AA5083, but for other samples as well, a comparable plateau in the 58–4.8 K range was seen before [20].

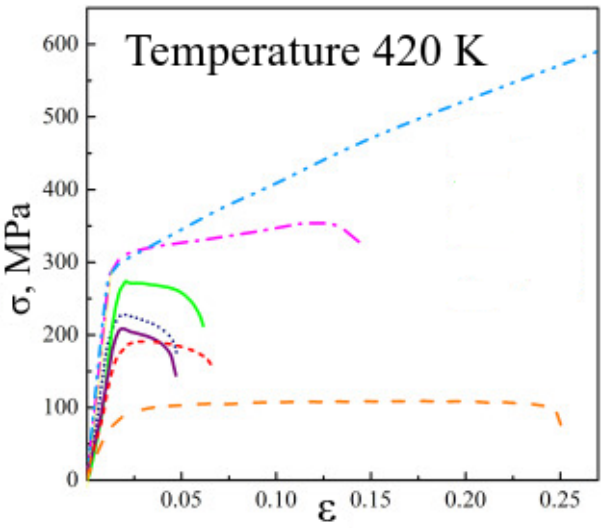

Figure 5. The true stress-true strain curves of ECAP of AA5083 [17].

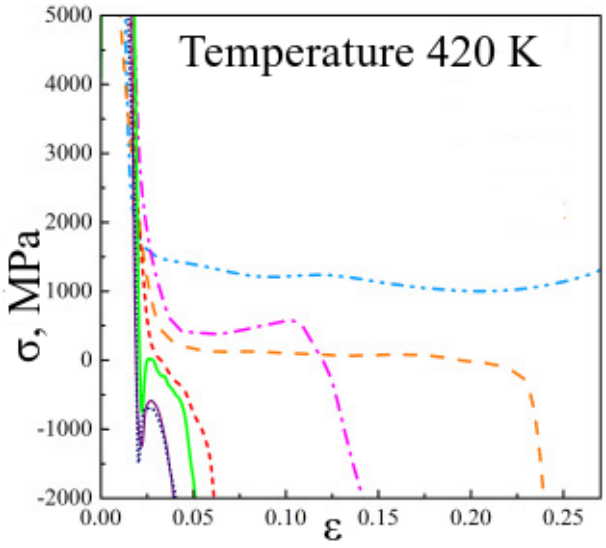

Figure 6. True strain curves and coefficient of strain hardening for ECAP AA5083 at different temperatures between 6.9 and 420 K [19].

3.1.2. Stress relaxation

Figure 7 is various depictions of stress relaxation curves obtained from experiments conducted at three distinct temperatures. It is evident that temperature plays a substantial role in influencing both the speed and extent of relaxation. As the temperature increases, both the rate and extent of relaxation at a given point during the

experiment experience an augmentation [21]. The stress relaxation curves observed in the experiments can be approximately modeled by the equation within the temperature range of 6.9 to 420 K [21].

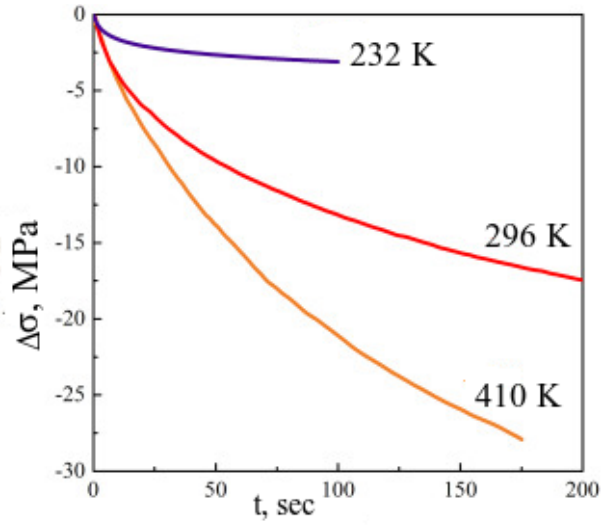

Figure 7. ECAP AA5083 at the same pre-strain (ε = 0.008) at 232, 296 and 410 K of the stress relaxation curves [22].

$$\Delta\sigma(t) = \alpha \ln(\beta t + 1) \tag{1}$$

where $\Delta\sigma(t)$ is the point at which the stress decreases from the beginning of relaxation to the point at which the relaxation parameter and stress are where $\alpha = \frac{kT}{V_s}$ and $\beta = \frac{M\varepsilon(0)}{\alpha}$. The activation volume $V_a(T)$ at a given strain, as inferred from the relaxation curves, governs the mechanisms that control the plastic deformity rate throughout a range of temperatures [22].

3.1.3. Microstructural evolution

The maps of inclination for the AA5083 specimens in their initial state of deformity are mentioned in **Figure 8**, based on the results of the EBSD measurements. The white and black lines represent low- and high-angle misorientation borders, respectively, while the colors of the grains represent different crystallographic orientations. LAGBs can be seen as a different structure in large grains, temperature effects during deformation at 310 and 125 K on the evolution of the microstructure. The initial structural distribution is bimodal, with individual grains up to 32 m in size and a typical grain size of 2.1 μm [23]. The average grain size d is decreased by tensile deformation of AA5083 following ECAP, although the largest grain sizes found after deformation at 310 and 125 K are 28 μm and 18 μm, respectively [23]. With deformation, the stronger the deformation, the particular fraction of large grains decreases with decreasing temperature and decreasing grain size. The pattern on the grain size chart transforms from having two peaks in a bimodal distribution seen in the original polycrystal and the one that underwent deformation at 125 K and 310 K, exhibiting a lognormal distribution that was later seen in the polycrystal shown in **Figure 8** [24].

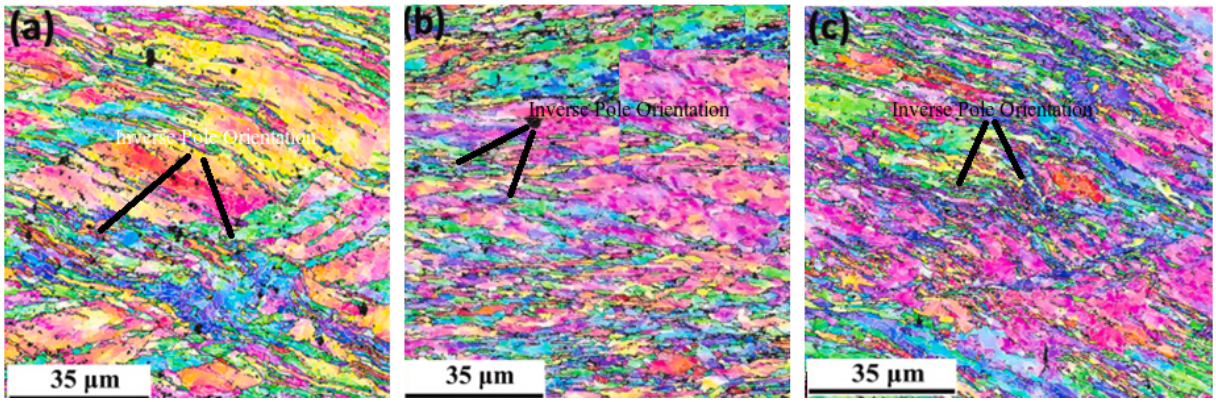

Figure 8. The EBSD orientation maps of AA8053 samples after ECAP before tension and after tension [24] such as: **(a)** Inverse pole orientation at 35 µm at initial stage; **(b)** Inverse pole orientation at 35 µm after tension; **(c)** Inverse pole orientation at 35 µm final stage.

Using the EBSD approach, it is possible to determine how the dislocation structure evolved by contrasting the kernel average misorientation maps of the AA5083 with respect to the deformity temperature before and after deformations. Low and high dislocation density are represented, respectively, by the regions with tiny and large KAM. The KAM for samples of the AA5083 material at 310 and 125 K both before and after deformation—the polycrystals first KAM map shows a high dislocation density, which is typical of the SPD of alloys made with AA5083 [25]. After being deformed at 125 K. The changes in the dislocation structure evolution process shown in **Figure 9**, when plastic deformation occurs at temperatures of 310 and 125 K, are qualitatively confirmed by the distributional features. KAM data can be used to estimate the density of dislocations that are geometrically required and is calculated as follows:

$$\rho = \frac{c\theta}{ub} \tag{2}$$

where θ and u are misorientation angle and distance used for evaluation of the misorientation angle. For microcrystalline AA5083 following low-temperature deformation, the GND density measurement is two orders of magnitude greater than the X-ray diffraction method's estimate.

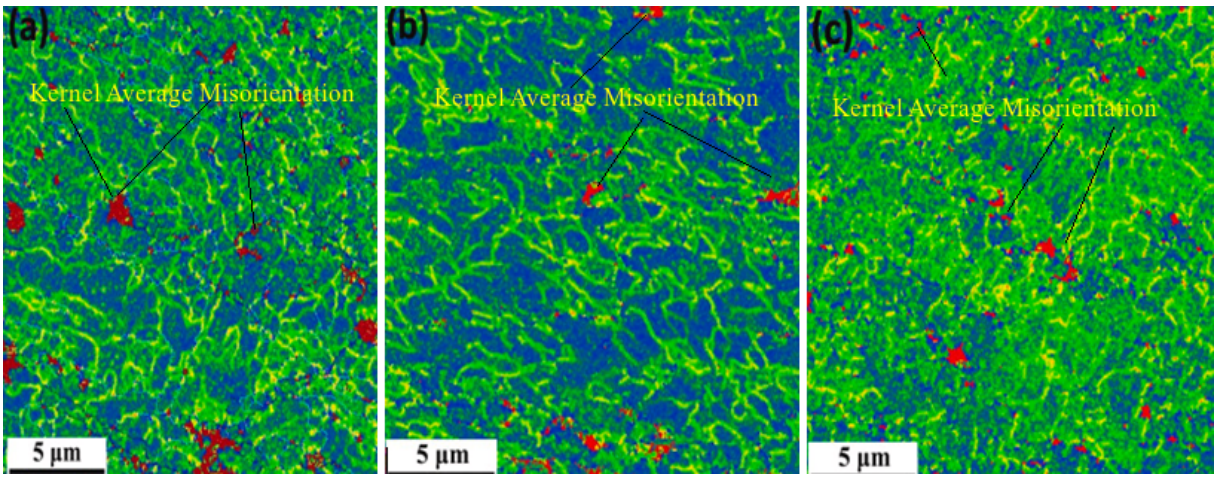

Figure 9. **(a)** AA5083 samples in initial state; **(b)** after tension at 310 K; **(c)** 125 K [26].

Similar microstructures are estimated differently, but this is perfectly acceptable

and can be explained by the different experimental techniques used to make these estimates [26]. An initial testing is a must before determining temperature values for the thermal treatments of this material. This investigation involves a comparison of hardness and aims to identify the temperature at which recrystallization occurs. After reaching the correct temperature, the samples were put in the oven to achieve. After each sample was heated for an hour at the specified temperature, its hardness was evaluated. The hardness data for the starting state and after two and four ECAP runs without heat treatment are shown in **Figure 10**. The enhancement in hardness after two ECAP passes, amounting to 69.1% compared to the material's initial state, does not undergo significant alteration with additional ECAP passes [27]. For instance, after four passes, the achieved improvement was 73.8%.

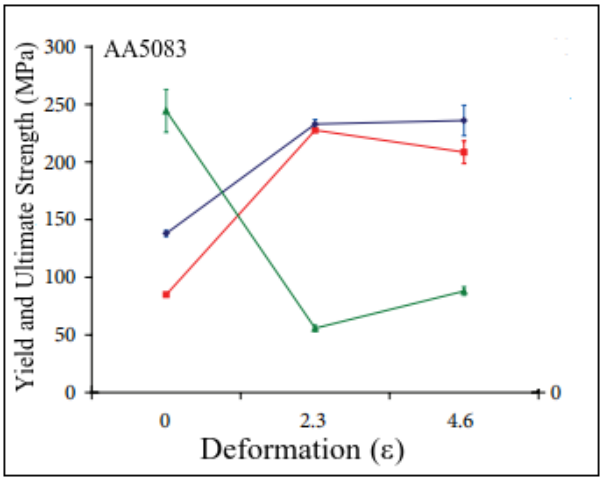

Figure 10. Variations in the mechanical properties, specifically S_y, S_{uts}, and ε of AA5083 as a function of the number of ECAP [27].

Similar results are found when accounting for the mechanical properties derived from the tensile testing. The elongation at failure decreases after two passes, while the yield stress and tensile strength increase. Owing to the effects of plastic strain saturation and work hardening, the properties acquired after four ECAP passes are identical to those obtained after two passes. **Table 1** is mentioned using the Vickers hardness scale, an overview of the values from the different samples under study [28]. The hardness values for each of the various heat treatments applied to the samples in the two ECAP states are shown in **Figure 11**. The final result is consistent with the hardness value that was recorded for the initial state. The hardness measurement obtained with two ECAP passes and without any heat treatment is represented by the upper line. The hardness experiences a slight increase potentially attributed to the variability of the hardness tester; there is a gradual decline in hardness starting from 470 K onwards [29]. The hardness becomes lower than the measurement for the initial state from 620 K upwards.

Afterward, for five of these temperatures (excluding the thermal treatment at 445 K due to its excessively low temperature), the samples underwent thermal treatment for varying holding times: 8 min, 34 min, 68 min, 102 min, 188 min, 308 min, and 428 min. Hardness tests, as well as optical and scanning electron microscopy, were conducted on these samples. **Figure 12** provides an overview of the hardness evolution resulting from

the performed treatments. Based on the obtained results, the thermal treatments at 470 K, 570 K, and 620 K were selected to conduct the tensile tests. Subsequently, these studies are presented in detail [31].

Table 1. Hardness measurements recorded for the AA5083 [30].

Deformation (ε)	**Temperature (K)**	**Time (minutes)**	**Hardness (HV)**
0	-	-	45
2.5	-	-	73
4.8	-	-	76
2.5	445	68	74
2.5	470	68	72
2.5	495	68	68
2.5	520	68	66
2.5	570	68	56
2.5	620	68	42

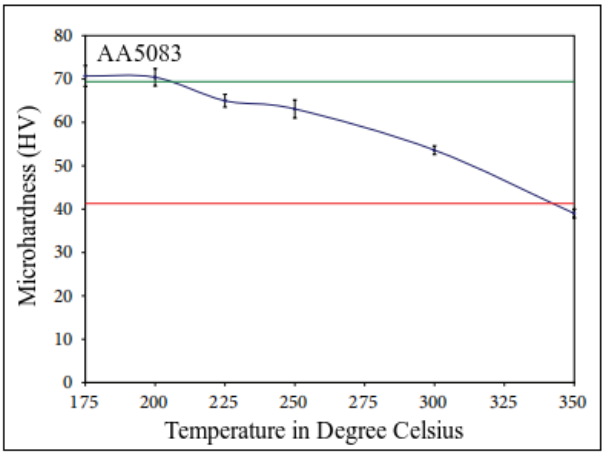

Figure 11. Hardness values for AA5083 two ECAP passes after one-hour thermal treatments at various temperatures [3].

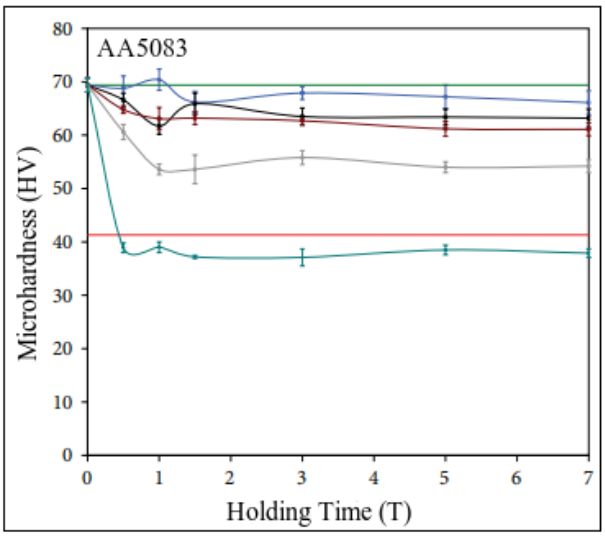

Figure 12. Hardness for AA5083 two ECAP passes in relation to the duration of holding time at 470 K, 495 K, 520 K, 570 K, and 620 K [32].

3.1.4. Thermal treatment at 470 K

In this current investigation, the optimal recovery temperature is defined as the one at which the AA5083 alloy processed by ECAP experiences a marginal reduction in hardness and simultaneously enhances its ductility through a specific thermal treatment [33].

As per the preceding section, the chosen optimal recovery temperature was 470 K. As shown in **Figure 13**, **Table 2** shows the measured hardness values for each holding duration at 470 K. Even after 428 min of treatment, the material's hardness does not significantly reduce. For the holding period of 68 min, a slight peak appears. Beyond this duration, the hardness starts to decrease slightly until it stabilizes around a value of approximately 68 HV. Considering these observations, three distinct holding times—8 min, 68 min, and 308 min—were chosen for conducting the tensile tests. The results obtained are presented in **Figure 14**. It can be inferred that the material's yield stress (S_y) and tensile strength stress (S_{uts}) diminish as the recovery thermal treatment holding time increases. Hence, it can be determined that for 68 min and 308 min of treatment, there is a reduction in the yield stress of 10.2% and 12.8%, respectively [34]. The decrease in tensile strength is approximately 4.8% for 68 min of treatment and 8.4% for 308 min of treatment, respectively. As anticipated, an augmentation in ductility is observed in comparison to the billet processed twice through ECAP. With a holding time of 68 min, this increase amounts to 16.8%, and in the case of 308 min, it is approximately 36%.

Table 2. Hardness values for AA5083 after varying holding times at 470 K [31].

Deformation (ε)	Temperature (K)	Time (minutes)	Hardness (HV)
2.5	470	-	74
2.5	470	34	76
2.5	470	68	74
2.5	470	102	70
2.5	470	180	71
2.5	470	180	72
2.5	470	420	70

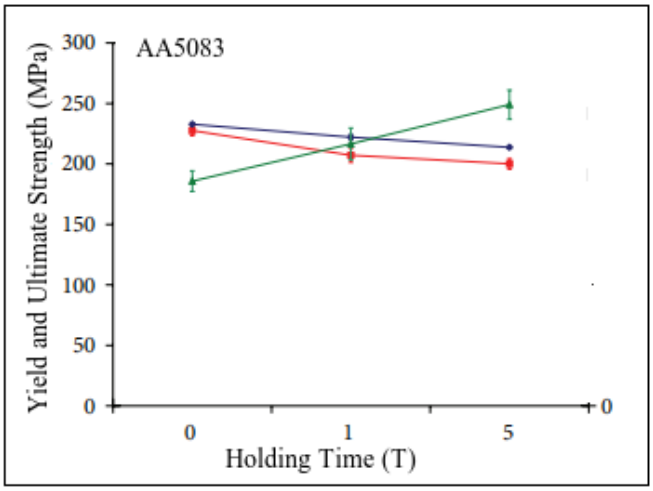

Figure 13. Mechanical properties S_y, S_{uts}, and ε for AA5083 two ECAP passes in relation to the holding time during the recovery thermal treatment at 470 K [33].

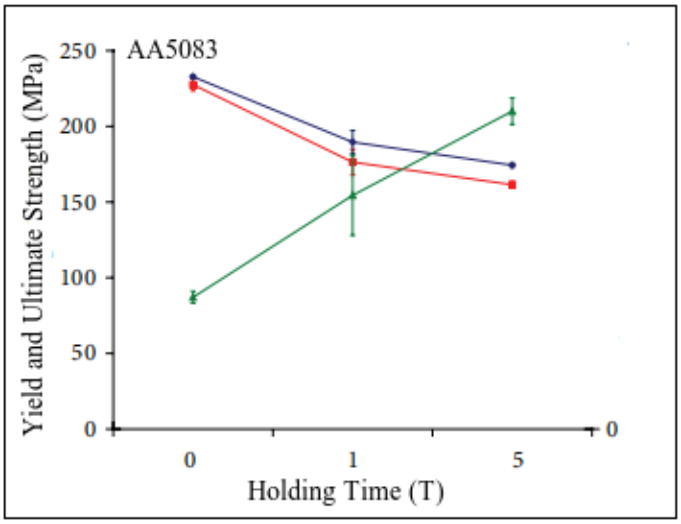

Figure 14. Mechanical properties S_y, S_{uts}, and ε for AA5083 two ECAP passes in relation to the holding time during an intermediate thermal treatment at 570 K [35].

3.1.5. Thermal treatment at 570 K

The temperature for this treatment was selected as it falls between the recovery and recrystallization temperatures of 620 K, serving as an intermediate point. As will be illustrated later, recrystallization does not occur even after a treatment duration of 428 minutes. Improving the qualities without sacrificing ductility is the goal of Wang and Huang [36]. As shown in **Figure 15**, **Table 3** shows the measured hardness values for each holding duration at 570 K. **Figure 15** indicates that the hardness experiences a 25% decrease in the first hour of treatment, reaching a value of 54.6 HV, after which it stabilizes or even exhibits a slight increase with longer durations. Following these findings, three distinct holding times—8 min, 68 min, and 308 min—were chosen to conduct the tensile tests. As the treatment's holding duration increases, the material's yield stress and tensile strength both decrease noticeably. Consequently, there is a reduction of 22.8% and 32% in the yield stress concerning holding times of 68 min and 308 min, respectively [37]. Additionally, there is a decrease of 18.4% in tensile strength for the 68 min treatment and a decrease of 25.4% in the case of the 308 min treatment. Nevertheless, the ductility improves in the treated material compared to the material processed twice by ECAP. With a holding time of 68 min, this increase amounts to 77.6%, and in the case of 308 min, it is approximately 142.1%.

Table 3. Hardness values for AA5083 after varying holding times at 570 K [38].

Deformation (ε)	Temperature (K)	Time (min)	Hardness (HV)
2.5	570	-	74
2.5	570	34	64
2.5	570	68	57
2.5	570	102	56
2.5	570	180	60
2.5	570	180	57
2.5	570	420	57

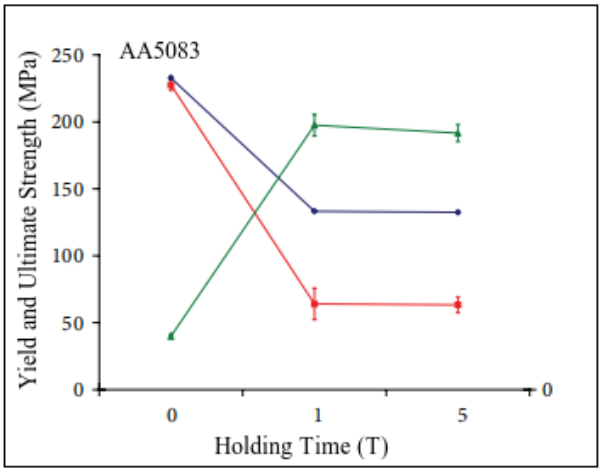

Figure 15. Mechanical properties S_y, S_{uts}, and ε for AA5083 two ECAP passes in relation to the holding time during the recrystallization thermal treatment at 620 K [39].

3.1.6. Thermal treatment at 620 K

A temperature of 620 K is chosen to facilitate better control of the recrystallization thermal treatment. A greater temperature would hasten the process of recrystallization as well as the reduction of hardness, causing the material's grain size to grow quickly. Reduction of grain size and improvement of ductility are the goals of this treatment. As indicated in **Table 4**, the hardness experiences a significant decrease during the initial hour of treatment, but in a manageable manner. The hardness values obtained at this 68-minute holding duration are lower than those obtained in the initial state of the material. Similar to previous sections, three distinct holding times—8 min, 68 min, and 380 min—were chosen to assess the mechanical properties. This was accomplished through the execution of multiple tensile tests, and the outcomes are presented in **Figure 16**.

Table 4. Hardness values for AA5083 after varying holding times at 620 K [40].

Deformation (ϵ)	Temperature (K)	Time (min)	Hardness (HV)
2.5	620	-	74
2.5	620	34	44
2.5	620	68	43
2.5	620	102	41
2.5	620	180	40
2.5	620	180	42
2.5	620	420	43

The material's tensile strength and yield stress both significantly decreased. Consequently, there is a reduction of 72.9% and 73.2% in the yield stress concerning holding times of 68 min and 308 min, respectively. A similar trend is observed in the tensile strength results, with a percentage decrease of 43.8% for 68 min and 44.1% for 308 min, respectively. Conversely, an enhancement in ductility is attained in the thermally treated material compared to the billet processed twice by ECAP. With a holding time of 68 min, this increase amounts to 398.1%, and in the case of 308 min, it is approximately 382.3%, as shown in **Figure 17**.

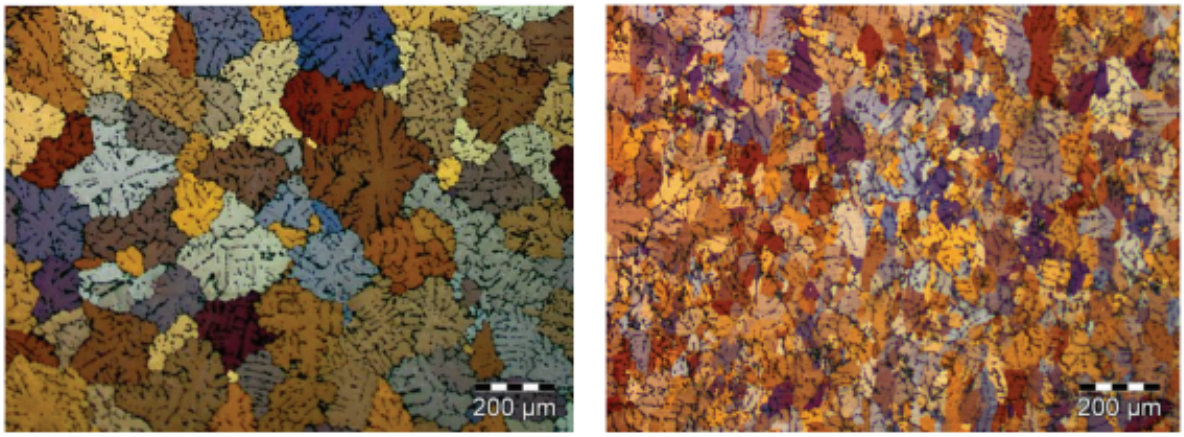

Figure 16. Initial material state and material processed twice with a thermal treatment at 620 K for 34 min [41].

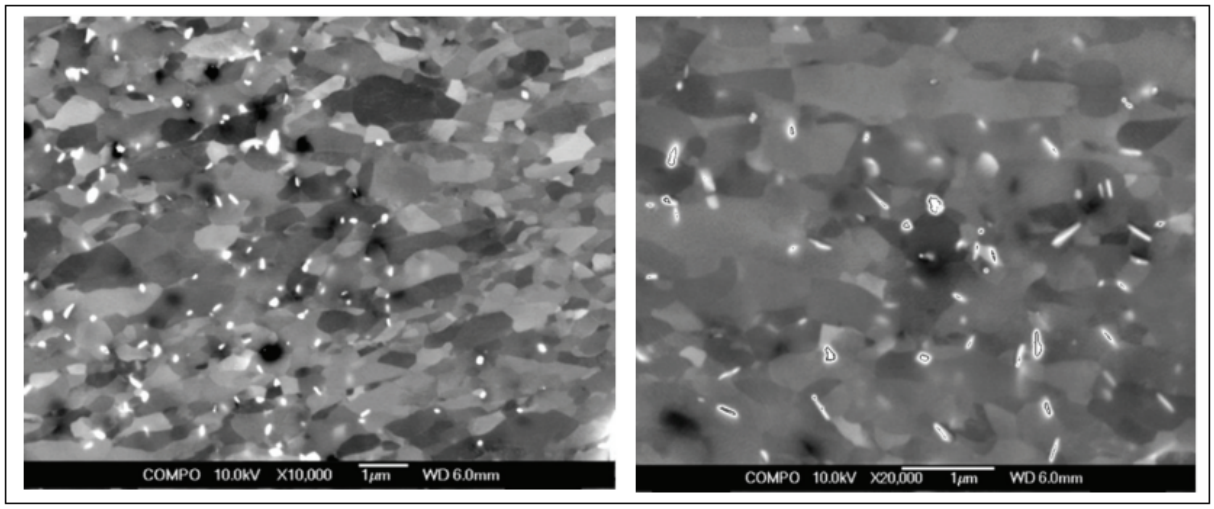

Figure 17. Microstructure after four ECAP passes [42].

4. Discussion

4.1. Plasticity of microcrystalline for AA5083

4.1.1. Influence of microstructure

To discover more about the microcrystalline AA5083's plastic deformation mechanics, extra crucial information on the microstructure studies before and after tension is obtained. A comprehensive examination using EBSD revealed that grain size reduction occurs across the entire size spectrum due to tensile deformation at both 125 K and 310 K. Another way to observe the alteration in grain size distribution due to deformation is by considering the extension of high-angle boundaries, which increased from 0.48 in the initial state to a range of 0.49–0.52 following the application of stress. The proportion of low-angle borders drops from 0.33 to 0.29–0.31. It is possible that during the deformation, dislocation rearrangement caused some of the low-angle boundaries to change into high-angle ones. During deformation, the impact of temperature on the development of the microstructure can be seen. Since the density of dislocations and the degree of microdeformation absolutely correspond with each other. The KAM value will alter if the microstructure changes under the impact

of specific factors [43]. The accumulation and interaction of dislocations result in deformity, which leads to the emergence of different configurations and a considerable increase in internal stresses and strains. Deformation lowers the dislocation density as well at room temperature. This demonstrates that the activation of dynamic recovery favors dislocation annihilation mechanisms over their accumulation during deformation at 310 K.

The values are tiny, between 125 and 310 K, compared to 410 K. The sample loses stability as a result of the sample's quick localization of deformity and the creation of necking, which results in a reduction in flow stress. In this temperature range, the least plasticity is shown [44]. According to a study of the structural components that affect how the neck develops. For lesser strains, the criterion for loss of stability will be met if the stress rises $\sigma < \theta$ while the coefficient of strain hardening stays the same. The coefficient of strain hardening and plasticity increases as a result of the slower diffusion dynamic processes that occur at lower temperatures, as seen in instance temperature at 82 K and 6.9 K. It is known that external dislocations at the borders cause sliding in certain materials.

4.1.2. Temperature effect

The relationship between yield strength $\sigma_{0.3}$ and temperature suggests that the thermally triggered mobility of dislocations through nearby impediments controls the speed at which a microcrystalline alloy deforms plastically at 82 K. The microcrystalline alloy has slope $\frac{d\sigma_{0.3}}{dT}$ and magnitude $\sigma_{0.2}$ that are greater than their corresponding values for the AA5083 [45]. Additionally, unlike the AA5083, for microcrystalline polycrystals, the dependency does not plateau between 165 and 310 K. The dependency on microcrystalline polycrystals never reaches a peak. It was demonstrated that for the AA5083 in the 48–150 K temperature range, plastic deformation rate and yielding strength occur when the attraction between grain dislocations and impurity atoms is thermally triggered. Due to the formation of crystal lattice defects, SPD in microcrystalline alloys results in a rise in internal and practical pressures versus AA5083. Internal tension is brought on by sliding dislocations' extensive interactions with grain boundaries. Due to other dislocations' elastic fields being thermally activated and having a weak dependence on temperature, they disappear at temperatures T_0 above a particular threshold, because moving dislocations encounter thermal barriers caused by the creation of additional high-angle boundaries. The threshold temperature T_0 of thermally induced plasticity and the barrier governing the rate of plastic deformation can both be evaluated using the suggested model. In order to clarify the dynamics of plastic deformation caused by heat fluctuation while dislocations are travelling through a system of similar short-range obstacles.

$$\left(\frac{\Delta\tau}{\Delta\ln\varepsilon}\right)_T = \tau_c(pqA)^{-1}\left(\frac{T}{T_0}\right)^{\frac{1}{q}}\left[1-\left(\frac{T}{T_0}\right)^{\frac{1}{q}}\right]^{\left(\frac{1-p}{p}\right)} \tag{3}$$

A number of conventional polycrystals have had their plastic deformation caused by mechanisms that have been identified using this theoretical model to successfully approximate experimental evidence. A coarse-grained alloy deforms plastically most

frequently in the temperature range of 6.9 to 148 K when impurity atoms are thermally activated and overcome by dislocations [46]. In estimating a microcrystalline alloy's experimental data, one was unable to determine precise acceptable thermally activated parameters of plastic deformation [46]. With the exception of the area around 6.9 K, the yield strength's temperature dependence is $\sigma_{0.2}$ across the whole temperature range. Additionally, in UFG polycrystals with complicated granular and intergranular microstructure and high dislocation density, there are multiple processes that can be combined to control how quickly thermally induced dislocations move.

4.1.3. Activation volume

The experimental determination of the activation volume V_a can be obtained through the analysis of stress relaxation data $V_a = \frac{MkT}{\alpha}$ using a correlation. Its nonmonotonic nature is one of the characteristics of $V_a(T)$ of the dependence of microcrystalline AA5083. The dependency of microcrystalline AA5083 has a nonmonotonic structure [47]. The intensification of the importance of grain boundaries during plastic deformation led to the involvement of numerous mechanisms [47]. As can be observed in **Figure 18**, the temperature range between 81 K and 220 K is increased by a significant amount varying from V_a. The values of V_a, the thermally induced forest dislocations intersection mechanism, can accept values of the variable's changing order. The measured values are a little lower and don't exactly match the forest dislocation intersection's basic mechanism. Volume V_a decreases as temperature rises up to $T \geq 220\ K$, the activation volume for aluminum's cross-slip, which is significantly less than the results of the investigation reported here. Higher values of V_a might result from the interaction of numerous thermally triggered mechanisms that regulate plastic deformity, such as cross slip, junction of forest dislocations, etc. The importance of interaction with its limits grows as the size of the grain or sub-grain diminishes [48].

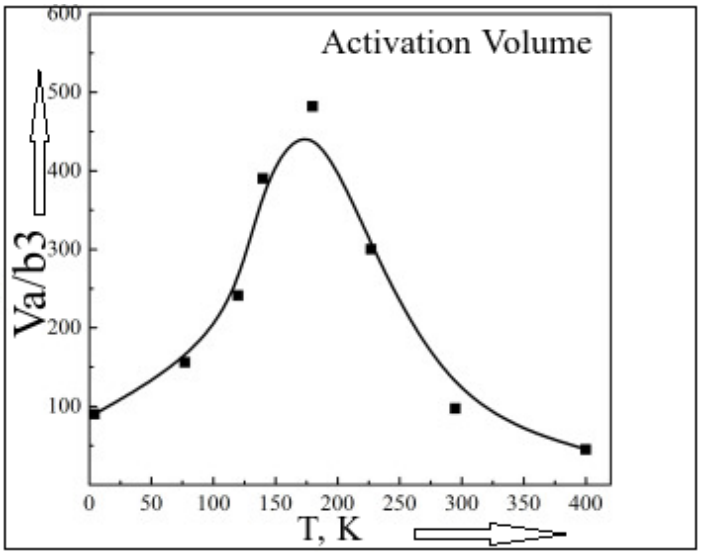

Figure 18. The activation volume V_a/b_3 is dependent on temperature [49].

This is brought on by a rise in the number of dislocations at grain borders and subboundaries. The development of a thick forest of dislocations close to cell walls and borders, as well as the requirement for unevenly distributed sources of dislocations.

As a result, an increase in dislocation activity inside boundary regions may also increase strain rate sensitivity [48]. A notable reduction in the activation volume for metals with ultrafine grains when compared to those with coarse grains. It may be assumed that it is feasible to superimpose several plastic deformation methods, resulting in the thermal activation parameters' values being averaged [49].

4.1.4. Recovery rate

When taking into account the recovery mechanisms, which are particularly noticeable at elevated temperatures and extensive deformation levels, an equation for stress relaxation was provided [50]. It is presumable that when under relaxation, internal stress σ_i rises according to deformation ε and falls proportionately to time t.

$$\Delta\sigma_i = \theta_a \Delta\varepsilon - r\Delta t \tag{4}$$

where $\theta_a = \left(\frac{d\sigma_i}{dt}\right)_{t,T}$ coefficient of strain hardening at the relaxation of the beginning, and $r = -\left(\frac{d\sigma_i}{dt}\right)_{t,T}$-recovery rate. At constant θ_a and r, the term describes the link between applied stress and downtime.

$$\Delta\sigma(t) = \frac{\alpha}{1+\theta_a/M} \ln\left[\varepsilon(0)M\left(1+\theta_a/M\right)\left(\frac{1}{r}\right)\left(\exp\left(\frac{r}{\alpha}\right)t - 1\right) + 1\right] \tag{5}$$

At brief moments of calm in case of a small value of r, the expression is closely related; with the passage of a very long duration, the relaxation curve anticipated by Equation (9) should eventually converge toward a linear slope $\frac{r}{(1+M\times\theta)}$. Finding the recovery rate in microcrystalline AA5083 requires approximating the relaxation curves using expression. The findings of such an evaluation are displayed in **Figure 19** [51]. At lower temperatures up to 220 K, the dependency is minimal (on the order of 5×10^{-3} MPa/s), and the relationship between *r* and temperature displays a limited degree of sensitivity [50].

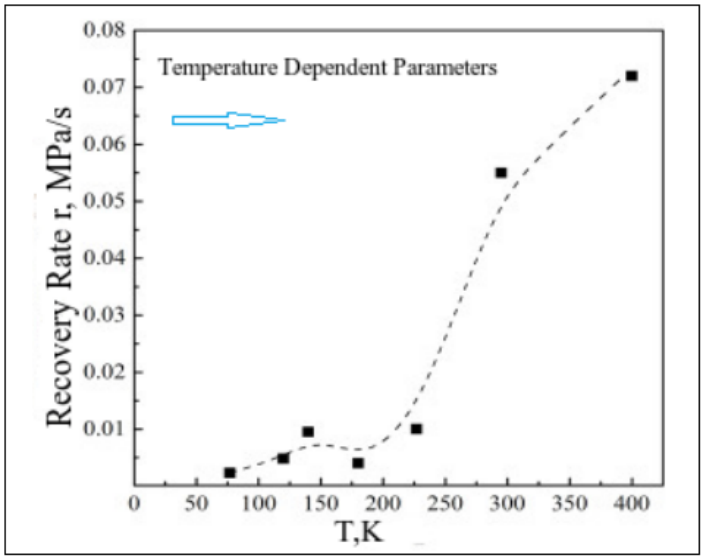

Figure 19. The recovery rate of microcrystalline AA5083 is temperature dependent [52].

Different stacking fault energies establish the cross-slip-related partial dislocations' splitting width. Cross-slip regulates the recovery mechanism at low and moderate temperatures [51]. Dislocation creep predominates at high temperatures because contact with voids is more obvious. In any event, dislocation annihilation reduces the dislocation density, and the speed at which this happens is determined by the energy barrier for annihilation, which also governs the associated recovery process [53]. The participation of both point faults and dislocations in the mechanism of recovery processes makes it difficult to explain [52]. The grain boundary diffusion coefficients for submicrocrystalline and nanocrystalline metals, as derived via SPD, were found to be bigger by several orders of magnitude than those for metals with coarse grains [53]. Consequently, the dynamic recovery process brought on by dislocation absorption in severely nonequilibrium boundaries even at a homologous temperature of 0.25 Celsius approximately, which is a pretty low temperature, when the circumstances for diffusion are much improved, Compared to typical coarse-grained polycrystals [54].

For a number of heat treatments, the refining grain that results from the buildup of various degrees of plastic strain will be displayed [54]. The starting material undergoes two ECAP passes via route C, is thermally treated during recrystallization to improve the grain size, and then undergoes two more ECAP runs by route [55]. The intermediate thermal treatment is conducted at 350 ℃ for a duration of 34 min, as depicted in **Figure 19**. When comparing the initial state with four passes, the grain refinement achieved in the material samples exceeds 260 times its initial grain size.

Additionally, the microstructure grains' size ratio has dropped to half of what it was previously. The enhancement of mechanical properties and uniformity is influenced by these two factors [55]. The outcomes are presented in **Table 5** [56]. The recovery rate of microcrystalline AA5083 is temperature dependent in **Figure 19** illustrates the grain size of the starting material, featuring an average value of 150 μm. In contrast, two ECAP passes with thermal treatment at 620 K for 34 min exhibit a reduced mean value of 50 μm [57]. Similarly, **Figure 20** displays a scanning electron microscope micrograph depicting the grain size of AA5083 after undergoing four equal channel angular pressing passes, with the billet rotated 180° between each ECAP pass designated as route C. Examining the Electron Backscatter Diffraction mapping, as illustrated in **Figure 20**, it becomes evident that the sample subjected to four passes exhibits significant grain misorientation, highlighted by noticeable differences in colors, aligning with expectations [58]. The corresponding histograms, depicted in **Figure 21**, are derived from the EBSD mapping results. The presented histogram illustrates the distribution function of grain size, centered around approximately 550 nm [58]. Additionally, the grain size ratio is depicted, with peaks falling within the range of 1.5 to 3.5.

Table 5. Sizes of grains and the ratio of grain sizes for various states of the AA5083 [59].

Deformation state	Grain size (μm)	Grain size ratio
N0 ($\varepsilon = 0$)	~160	> 8
N0 ($4.8 = 0$)	~1.6	~4.45

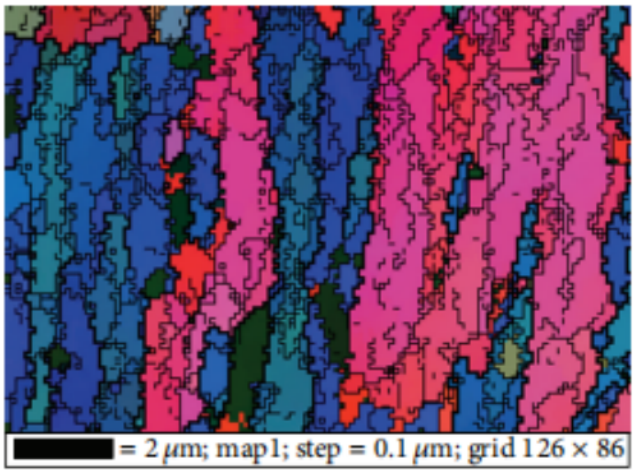

Figure 20. EBSD mapping of four passes [59].

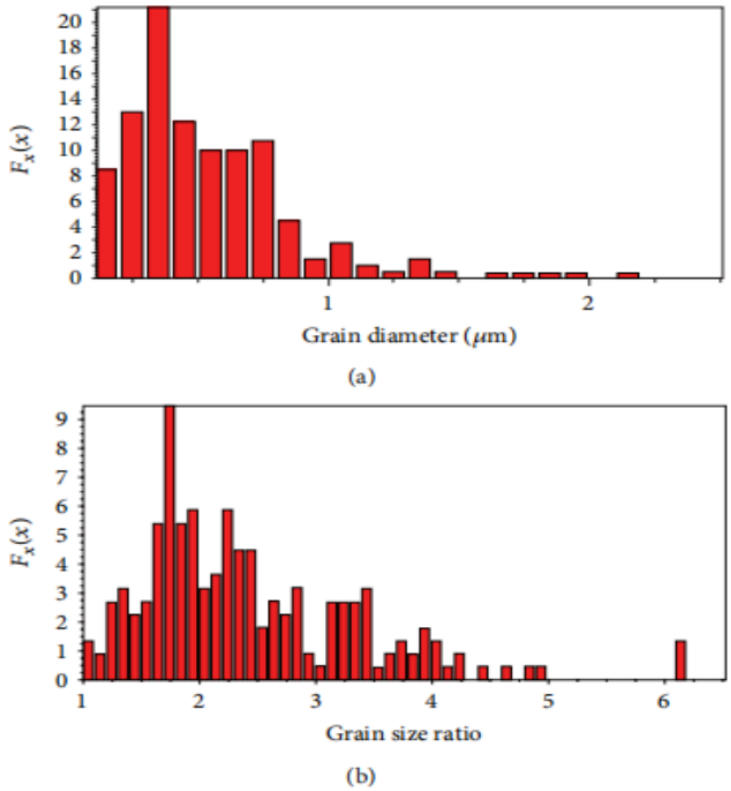

Figure 21. **(a)** Histogram showing the grain size and **(b)** Grain size ratio distribution functions for the four-pass sample [60].

To assess whether there is a reduction in the grain size value between the initial, two-pass, and four-pass states, **Figure 21** exhibits two scanning electron microscope micrographs illustrating the microstructures grain size. As is evident, there is not a substantial alteration in grain size when compared to the four-pass state, as illustrated in **Figure 22** [60]. The material was deformed over the course of four passes, arriving at a plastic deformation value of 4.8. Initially, the grain size was approximately 160 μm, and eventually, a grain size smaller than 1.2 μm was attained [61]. Conversely, the initial and two ECAP passes underwent initial processing through ECAP for two cycles, introducing a plastic strain of 2.5, and subsequently underwent a thermal treatment [61].

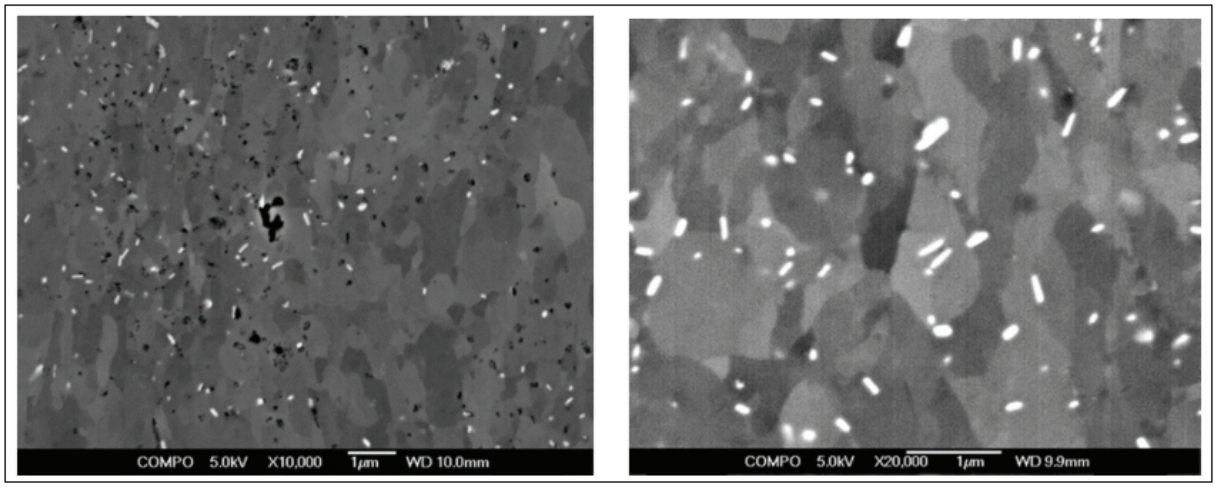

(a) **(b)**

Figure 22. Microscopic arrangement as: **(a)** the processing of the material in the initial; **(b)** two ECAP passes is stated [62].

Subsequently, the grain size underwent alterations, and the plastic strain was eliminated as a result of the treatment. The grain size measured approximately 50 μm [62]. Subsequently, this novel material underwent an additional two rounds of processing through ECAP, reaching a plastic deformation of 2.5. For this example, the starting grain size was about 50 μm, while the final grain size was less than 1.2 μm. All the materials had different beginning grain sizes and experienced plastic deformation up to a specific degree [63]. The experiment reveals that a decrease in the initial grain size correlates with a reduced amount of necessary plastic strain to achieve the targeted grain reduction. The diminished ductility observed in the temperature range of 125–310 K can be attributed to the lower rate of strain hardening, which is a result of the increased dynamic recovery within the microcrystalline alloy. This is the case despite the fact that the power and abundance of such barriers are significantly increased following severe plastic deformation [63].

5. Conclusion

The evolution of the microstructure in microcrystalline AA5083 subjected to ECAP was investigated through scanning electron microscopy in its initial state, as well as stress at a consistent strain rate at temperatures of 310 K and 125 K. The observations reveal the presence of a mixed grain structure characterized by a substantial dislocation density within grain boundaries. This structure consists of numerous grains with dimensions around 1.2 μm, alongside individual larger grains measuring approximately 12 μm. Under tensile deformation, the microcrystalline AA5083 tends to exhibit a reduction in the average grain size. At 125 K, deformation leads to a rise in the dislocation density within the grains. It has been demonstrated that the fundamental shape of the tension curves undergoes changes as the temperature decreases. A high dislocation density and non-equilibrium grain boundaries, which amplified recovery processes, are the causes of thermally induced plasticity. In this research, an investigation into the changes in microstructure and mechanical properties

was conducted on the aluminum alloy AA5083. The study involved subjecting the material to severe plastic deformation, utilizing the equal channel angular pressing process. It was established that employing a thermal treatment at 470 K with a dwell time of either 68 minutes or 308 minutes can lead to a notable enhancement in the mechanical properties. An increase of approximately 135% in yield stress can be achieved. This is highly relevant for the advancement of applications that demand excellent resistance properties.

Funding: This work received no external funding.

Conflict of interest: The authors declare no conflict of interest.

References

1. Zhao YH, Bingert JF, Topping TD, et al. Mechanical behavior, deformation mechanism and microstructure evolutions of ultrafine-grained Al during recovery via annealing. Materials Science and Engineering: A. 2020; 772: 138706. doi: 10.1016/j.msea.2019.138706
2. Zhu YT, Liao XZ, Wu XL. Deformation twinning in nanocrystalline materials. Progress in Materials Science. 2012; 57(1): 1–62. doi: 10.1016/j.pmatsci.2011.05.001
3. Singh N, Agrawal MK, Saxena KK, et al. Advancement and influence of designing of ECAP on deformation and microstructure properties of the AA5083 under thermal effects. International Journal on Interactive Design and Manufacturing (IJIDeM). 2023; 18(3): 1809–1827. doi: 10.1007/s12008-023-01213-y
4. Feltham P. Stress Relaxation in Magnesium at Low Temperatures. Physica Status Solidi (B). 1963; 3(8): 1340–1346. doi: 10.1002/pssb.19630030805
5. Pustovalov VV, Fomenko VS. Plastic Deformation of Crystals at Low Temperatures. Naukova Dumka, Kyiv; 2012.
6. Kocks UF, Argon AS, Ashby ME. Thermodynamics and Kinetics of Slip. In: Progress in Materials Science. Pergamon Press Oxford; 1975.
7. Chen J, Lu L, Lu K. Hardness and strain rate sensitivity of nanocrystalline Cu. Scripta Mater. 2006; 54: 1913–1918. doi: 10.1016/j.scriptamat.2006.02.022
8. Cahn RW, Haasen P. Physical Metallurgy. NorthHolland; 1983.
9. Conrad H, Yang D. Plastic deformation kinetics of electrodeposited Cu foil at low and intermediate homologous temperatures. Journal of Electronic Materials. 2002; 31(4): 304–312. doi: 10.1007/s11664-002-0148-x
10. Bonneville J, Escaig B, Martin JL. A study of cross-slip activation parameters in pure copper. Acta Metall. 1988; 36(8): 1989–2002.
11. Hoseini M, Hamid Pourian M, Bridier F, et al. Thermal stability and annealing behaviour of ultrafine grained commercially pure titanium. Materials Science and Engineering: A. 2012; 532: 58–63. doi: 10.1016/j.msea.2011.10.062
12. Hajizadeh K, Ghobadi Alamdari S, Eghbali B. Stored energy and recrystallization kinetics of ultrafine grained titanium processed by severe plastic deformation. Physica B: Condensed Matter. 2013; 417: 33–38. doi: 10.1016/j.physb.2013.02.031
13. Dyakonov GS, Mironov S, Semenova IP, et al. EBSD analysis of grain-refinement mechanisms operating during equal-channel angular pressing of commercial-purity titanium. Acta Materialia. 2019; 173: 174–183. doi: 10.1016/j.actamat.2019.05.014
14. Podolskiy AV, Ng HP, Psaruk IA, et al. Cryogenic equal channel angular pressing of commercially pure titanium: microstructure and properties. Journal of Materials Science. 2014; 49(19): 6803–6812. doi: 10.1007/s10853-014-8382-1
15. Tesař K, Jäger A. Electron backscatter diffraction analysis of the crack development induced by uniaxial tension in commercially pure titanium. Materials Science and Engineering: A. 2014; 616: 155–160. doi: 10.1016/j.msea.2014.08.028
16. Haušild P, Materna A, Nohava J. Characterization of Anisotropy in Hardness and Indentation Modulus by Nanoindentation. Metallography, Microstructure, and Analysis. 2013; 3(1): 5–10. doi: 10.1007/s13632-013-0110-8

17. Tuninetti V, Jaramillo AF, Riu G, et al. Experimental Correlation of Mechanical Properties of the Ti-6Al-4V Alloy at Different Length Scales. Metals. 2021; 11(1): 104. doi: 10.3390/met11010104
18. Palán J, Kubina T, Motyčka P. The effect of annealing on mechanical and structural properties of UFG titanium grade 2. IOP Conference Series: Materials Science and Engineering. 2017; 179: 012055. doi: 10.1088/1757-899x/179/1/012055
19. Oberdorfer B, Steyskal EM, Sprengel W, et al. Recrystallization kinetics of ultrafine-grained Ni studied by dilatometry. Journal of Alloys and Compounds. 2011; 509: S309–S311. doi: 10.1016/j.jallcom.2010.12.130
20. Seiner H, Bodnárová L, Sedlák P, et al. Application of ultrasonic methods to determine elastic anisotropy of polycrystalline copper processed by equal-channel angular pressing. Acta Materialia. 2010; 58(1): 235–247. doi: 10.1016/j.actamat.2009.08.071
21. Evans JA, Sturtevant BT, Clausen B, et al. Determining elastic anisotropy of textured polycrystals using resonant ultrasound spectroscopy. Journal of Materials Science. 2021; 56(16): 10053–10073. doi: 10.1007/s10853-021-05827-z
22. Kube CM, Gillespie J, Cherry M. Influence of residual stress and texture on the resonances of polycrystalline metals. The Journal of the Acoustical Society of America. 2021; 150(4): 2624–2634. doi: 10.1121/10.0006667
23. Sedlák P, Seiner H, Zídek J, et al. Determination of All 21 Independent Elastic Coefficients of Generally Anisotropic Solids by Resonant Ultrasound Spectroscopy: Benchmark Examples. Experimental Mechanics. 2014; 54(6): 1073–1085. doi: 10.1007/s11340-014-9862-6
24. Nejezchlebová J, Janovská M, Seiner H, et al. The effect of athermal and isothermal ω phase particles on elasticity of β-Ti single crystals. Acta Materialia. 2016; 110: 185–191. doi: 10.1016/j.actamat.2016.03.033
25. Nejezchlebová J, Seiner H, Sedlák P, et al. On the complementarity between resistivity measurement and ultrasonic measurement for in-situ characterization of phase transitions in Ti-alloys. Journal of Alloys and Compounds. 2018; 762: 868–872. doi: 10.1016/j.jallcom.2018.05.173
26. Nejezchlebová J, Janovská M, Sedlák P, et al. Elastic constants of β-Ti15Mo. Journal of Alloys and Compounds. 2019; 792: 960–967. doi: 10.1016/j.jallcom.2019.03.418
27. Janovskaa M, Nejezchlebova J, Sedlak P, et al. Elastic constants of Ti-15Mo single crystals and their evolution with thermal treatment. MATEC Web of Conferences. 2020; 321: 12012. doi: 10.1051/matecconf/202032112012
28. Vokoun D, Maňák J, Tesař K, et al. Compression of ecaped titanium micro-pillars for two principal orientations. Acta Polytechnica CTU Proceedings. 2020; 27: 1–5. doi: 10.14311/app.2020.27.0001
29. Tesař K, Gärtnerová V, Němec M, et al. Fe-stabilized duplex α/β microstructure containing γ titanium hydride in Ti grade 2 obtained by volumetrically incomplete phase transition. Materials Characterization. 2019; 153: 128–135. doi: 10.1016/j.matchar.2019.04.045
30. Koller M, Sedlák P, Seiner H, et al. An ultrasonic internal friction study of ultrafine-grained AZ31 magnesium alloy. Journal of Materials Science. 2014; 50(2): 808–818. doi: 10.1007/s10853-014-8641-1
31. Oliver WC, Pharr GM. Measurement of hardness and elastic modulus by instrumented indentation: Advances in understanding and refinements to methodology. Journal of Materials Research. 2004; 19(1): 3–20. doi: 10.1557/jmr.2004.19.1.3
32. Mendelson MI. Average Grain Size in Polycrystalline Ceramics. Journal of the American Ceramic Society. 1969; 52(8): 443–446. doi: 10.1111/j.1151-2916.1969.tb11975.x
33. Sopha H, Tesar K, Knotek P, et al. TiO2 nanotubes grown on Ti substrates with different microstructure. Materials Research Bulletin. 2018; 103: 197–204. doi: 10.1016/j.materresbull.2018.03.036
34. Yu Q, Shan ZW, Li J, et al. Strong crystal size effect on deformation twinning. Nature. 2010; 463(7279): 335–338. doi: 10.1038/nature08692
35. Ghaderi A, Barnett MR. Sensitivity of deformation twinning to grain size in titanium and magnesium. Acta Materialia. 2011; 59(20): 7824–7839. doi: 10.1016/j.actamat.2011.09.018
36. Wang YN, Huang JC. Texture analysis in hexagonal materials. Materials Chemistry and Physics. 2003; 81: 11–26. doi: 10.1016/S0254-0584(03)00168-8
37. Zel'dovich VI, Frolova NY, Patselov AM, et al. The ω-phase formation in titanium upon deformation under pressure. The Physics of Metals and Metallography. 2010; 109(1): 30–38. doi: 10.1134/s0031918x10010059
38. Hennig RG, Trinkle DR, Bouchet J, et al. Impurities block the α to ω martensitic transformation in titanium. Nature Materials. 2005; 4(2): 129–133. doi: 10.1038/nmat1292
39. Todaka Y, Sasaki J, Moto T, et al. Bulk submicrocrystalline ω-Ti produced by high-pressure torsion straining. Scripta Materialia. 2008; 59(6): 615–618. doi: 10.1016/j.scriptamat.2008.05.015

40. Sajadifar SV, Atli C, Yapici GG. Effect of severe plastic deformation on the damping behavior of titanium. Materials Letters. 2019; 244: 100–103. doi: 10.1016/j.matlet.2019.02.010
41. Singh N, Agrawal MK, Verma SK, et al. Study of the effect of ECAPed Method on the Mechanical Properties of AA 5083: An Overview. International Research Journal on Advanced Science Hub. 2022; 4(6): 186–191. doi: 10.47392/irjash.2022.044
42. Koller M, Chráska T, Cinert J, et al. Mechanical and magnetic properties of semi-Heusler/light-metal composites consolidated by spark plasma sintering. Materials & Design. 2017; 126: 351–357. doi: 10.1016/j.matdes.2017.04.028
43. Conrad H. Thermally activated deformation of α titanium below 0.4 TM. Canadian Journal of Physics. 1967; 45(2): 581–590. doi: 10.1139/p67-050
44. Liu X, Zhang Q, Zhao X, et al. Ambient-temperature nanoindentation creep in ultrafine-grained titanium processed by ECAP. Materials Science and Engineering: A. 2016; 676: 73–79. doi: 10.1016/j.msea.2016.08.111
45. Sotniczuk A, Kuczyńska-Zemła D, Królikowski A, et al. Enhancement of the corrosion resistance and mechanical properties of nanocrystalline titanium by low-temperature annealing. Corrosion Science. 2019; 147: 342–349. doi: 10.1016/j.corsci.2018.11.016
46. Zhao PC, Chen B, Zheng ZG, et al. Microstructure and Texture Evolution in a Post-dynamic Recrystallized Titanium During Annealing, Monotonic and Cyclic Loading. Metallurgical and Materials Transactions A. 2020; 52(1): 394–412. doi: 10.1007/s11661-020-06071-x
47. Zhao P, Chen B, Kelleher J, et al. High-cycle-fatigue induced continuous grain growth in ultrafine-grained titanium. Acta Materialia. 2019; 174: 29–42. doi: 10.1016/j.actamat.2019.05.038
48. Bozzolo N, Dewobroto N, Grosdidier T, et al. Texture evolution during grain growth in recrystallized commercially pure titanium. Materials Science and Engineering: A. 2005; 397(1–2): 346–355. doi: 10.1016/j.msea.2005.02.049
49. Wang Y, He W, Liu N, et al. Effect of pre-annealing deformation on the recrystallized texture and grain boundary misorientation in commercial pure titanium. Materials Characterization. 2018; 136: 1–11. doi: 10.1016/j.matchar.2017.11.059
50. Fisher ES, Renken CJ. Single-Crystal Elastic Moduli and the hcp → bcc Transformation in Ti, Zr, and Hf. Physical Review. 1964; 135(2A): A482–A494. doi: 10.1103/physrev.135.a482
51. Singh N, Agrawal MK, Verma SK, et al. A Review on Effect of Stress and Strain Distribution on the AA5083 With Respect to Different Channel Angle of ECAP. International Research Journal on Advanced Science Hub. 2022; 4(3): 57–66. doi: 10.47392/irjash.2022.013
52. Pilz S, Gustmann T, Günther F, et al. Controlling the Young's modulus of a ß-type Ti-Nb alloy via strong texturing by LPBF. Materials & Design. 2022; 216. doi: 10.1016/j.matdes.2022.110516
53. Majumdar P, Singh SB, Chakraborty M. Elastic modulus of biomedical titanium alloys by nano-indentation and ultrasonic techniques—A comparative study. Materials Science and Engineering: A. 2008; 489(1–2): 419–425. doi: 10.1016/j.msea.2007.12.029
54. Materna A, Haušild P, Nohava J. A Numerical Investigation of the Effect of Cubic Crystals Orientation on the Indentation Modulus. Acta Physica Polonica A. 2015; 128(4): 693–697. doi: 10.12693/aphyspola.128.693
55. Abbasi M, Ahmadi F, Farzin M. Production of Ultrafine-Grained Titanium with Suitable Properties for Dental Implant Applications by RS-ECAP Process. Metals and Materials International. 2020; 27(4): 705–716. doi: 10.1007/s12540-020-00796-5
56. Singh N, Agrawal MK, Verma SK, et al. A review on impact route process on AA5083 of back pressure through equal channel angular pressing. Materials Today: Proceedings. 2023. doi: 10.1016/j.matpr.2023.08.163
57. Singh N, Agrawal MK. Deformation Behaviour of the Billet and Tooling Design on AA5083 through Equal Channel Angular Pressing with Effect of Back Pressure. Journal of Polymer & Composites. 2024; 12(Special Issue 1): S287–S303.
58. Barnes AJ. Superplastic Aluminum Forming - Expanding Its Techno-Economic Niche. Materials Science Forum. 1999; 304–306: 785–796. doi: 10.4028/www.scientific.net/msf.304-306.785
59. Ma ZY, Mishra RS. Cavitation in superplastic 7075Al alloys prepared via friction stir processing. Acta Mater. 2003; 51(12): 3551–3569. doi: 10.1016/S1359-6454(03)00173-3
60. Chokshit AH, Mukherjee AK. An analysis of cavity nucleation in superplasticity. Acta Metall. 1989; 37(11): 3007–3017. doi: 10.1016/0001-6160(89)90337-4
61. Friedman PA, Ghosh AK. Microstructural evolution and superplastic deformation behavior of fine grain 5083Al. Metallurgical and Materials Transactions A. 1996; 27(12): 3827–3839. doi: 10.1007/bf02595632

62. Bae DH, Ghosh AK. Cavity growth in a superplastic Al–Mg alloy: II. An improved plasticity based model. Acta Mater. 2002; 50(5): 1011–1029. doi: 10.1016/S1359-6454(01)00400-1
63. Shin DH, Kim BC, Kim YS, et al. Microstructural evolution in a commercial low carbon steel by equal channel angular pressing. Acta Mater. 2000; 48(9): 2247–2255. doi: 10.1016/S1359-6454(00)00028-8